Radio Frequency Induced Heating of a Medical Device with Vascular Flow Conditions

Benjamin W. Scandling

Table of Contents

Chapter 1: Abstract

Magnetic Resonance Imaging (MRI) is a tool used to scan more than 40 million U.S. patients every year, but a major concern exists with the safety of patients with implanted medical devices. When implanted medical devices constructed of electrically conductive materials are subjected to an oscillating magnetic field, electric currents are produced according to Faraday's Law of Induction. These electric currents cause potentially damaging Radio Frequency (RF) induced heating near the device. The current standard test method, ASTM F2182, for evaluating MR safety of medical devices defines the use of a phantom consisting of a gel with thermal and electrical properties that approximate tissue and does not incorporate convective blood flow. It was hypothesized that vascular flow would cause a significant reduction in RF induced heating during MRI. An ASTM phantom was modified to include a flow channel and a Zilver 635® Vascular Self-Expanding Stent within the channel. Experiments were performed in a Siemens 3-Tesla MRI system. Flow rate was varied from 0 to 2240 mL/min and transient temperatures were measured using fiber optic probes. It was found that constant flow significantly reduced the maximum temperature increase when the device was subjected to MRI-powered RF induced heating. The maximum temperature rise measured approximately 10°C without flow, while physiologic flow rates decreased temperature rises by up to 70%. These experimental results were used to validate a COMSOL MultiPhysics® simulation which was in agreement with the experimental data over the physiological range of flow. The agreement shows that the simulation can be utilized to accurately predict the influence of blood flow on RF induced heating of a vascular stent. The results of this study indicate that blood flow has a significant cooling effect and support the use of simulation tools to predict device heating under physiological conditions. These results will hopefully lead to more accurate evaluation of the MR safety of medical devices with the goal of ensuring that patients with unsafe devices are precluded from MRI scans, and those with safe devices have access to clinically indicated MRI scans.

Chapter 2: Introduction

An estimated 85.6 million Americans have at least one form of cardiovascular disease, and this disease has been the leading cause of death in the United States for every year since 1919 [1]. A common symptom of cardiovascular diseases is the blockage and possible complete closure of blood vessels throughout the body. To treat blocked vessels, physicians repair them with a process known as angioplasty where a stent is deployed to keep the vessel open for an extended period of time [2]. After surgical repair, patients will require constant monitoring, often through the use of various medical imaging modalities. One of these modalities is magnetic resonance imaging (MRI) and it is a very powerful tool used to analyze and diagnose patients with different types and stages of cardiovascular disease. MRI is widely regarded as a safe medical procedure as it provides images of any part of the human body without the use of invasive procedures or damaging ionizing radiation. However, there are concerns about the safety of conducting MRI scans on patients with implanted medical devices. Metallic medical devices such as vascular stents used in angioplasty are electrically conductive and are susceptible to electric currents inside the magnetic bore. These currents cause radio frequency (RF) induced heating near the device which could damage both the device and the surrounding tissue [3]. To warn patients, radiologists, and MRI technologists of the possible dangers, the American Society of Testing and Materials (ASTM) has created labels for medical devices and their general safety in the MR environment. A device can be "MR Safe" if it poses no known hazards, "MR Conditional" if it poses no known hazards under specified conditions, or "MR Unsafe" if it poses hazards. Metallic devices, such as vascular stents, are typically labelled as "MR Conditional" and require testing to determine what conditions they can be safely scanned in [4]. ASTM has also developed standardized test methods to evaluate MR safety of these types of devices. However, these standards do not account for physiological effects, such as blood flow and perfusion. Blood flow is an important thermodynamic factor to be considered because flow (i.e., fluid dynamics) can significantly impact the overall temperature rise by accounting for convective heat transfer. It is believed that convective heat transfer can drastically change the evaluation of medical

devices that can be considered “MR Conditional”. Due to the neglect of convective heat transfer, it was hypothesized that the currently accepted standard test methods over-estimate the temperature rise of medical devices in vivo, and therefore may unnecessarily exclude patients from MRI procedures.

Along with an elevated temperature, the time of tissue exposure at increased temperatures is of concern. Exposure to temperatures at or above 42.5°C [31] can lead to non-reversible change or damage. This value was used to quantify the amount of exposure a tissue receives at higher temperatures in terms of minutes. Cumulative Equivalent Minutes spent at 43°C (CEM43) is calculated by:

$$CEM_{43} = \sum_{t=0}^{t=final} R^{43-T}\Delta t \qquad \text{with } R = \begin{cases} 0.25 & T < 43\ ^\circ C \\ 0.50 & T \geq 43\ ^\circ C \end{cases} \qquad [1]$$

where R is tissue thermal sensitivity, T is temperature at a given time t between measurements [32]. CEM43 values can give an accurate estimation of exposure to RF induced heating during MRI [32].

Based on normal cardiac output, blood flows through the body at a total rate of around 5 L/min at rest [20]. This study will measure the cooling effect of flow within the physiological range (0 to 5 L/min) on RF induced heating. The stent utilized in this study is indicated for the iliac artery which has a flow of approximately 350 mL/min [16]. Flow throughout the rest of the body is similar in magnitude to this value and approximate values for other vessels are shown in figure 1. The vessels shown in figure 1 are commonly stented and would experience RF induced temperature rises as discussed in this study. However, each vessel and case requires stents of different geometries and therefore, temperature rises will have variations.

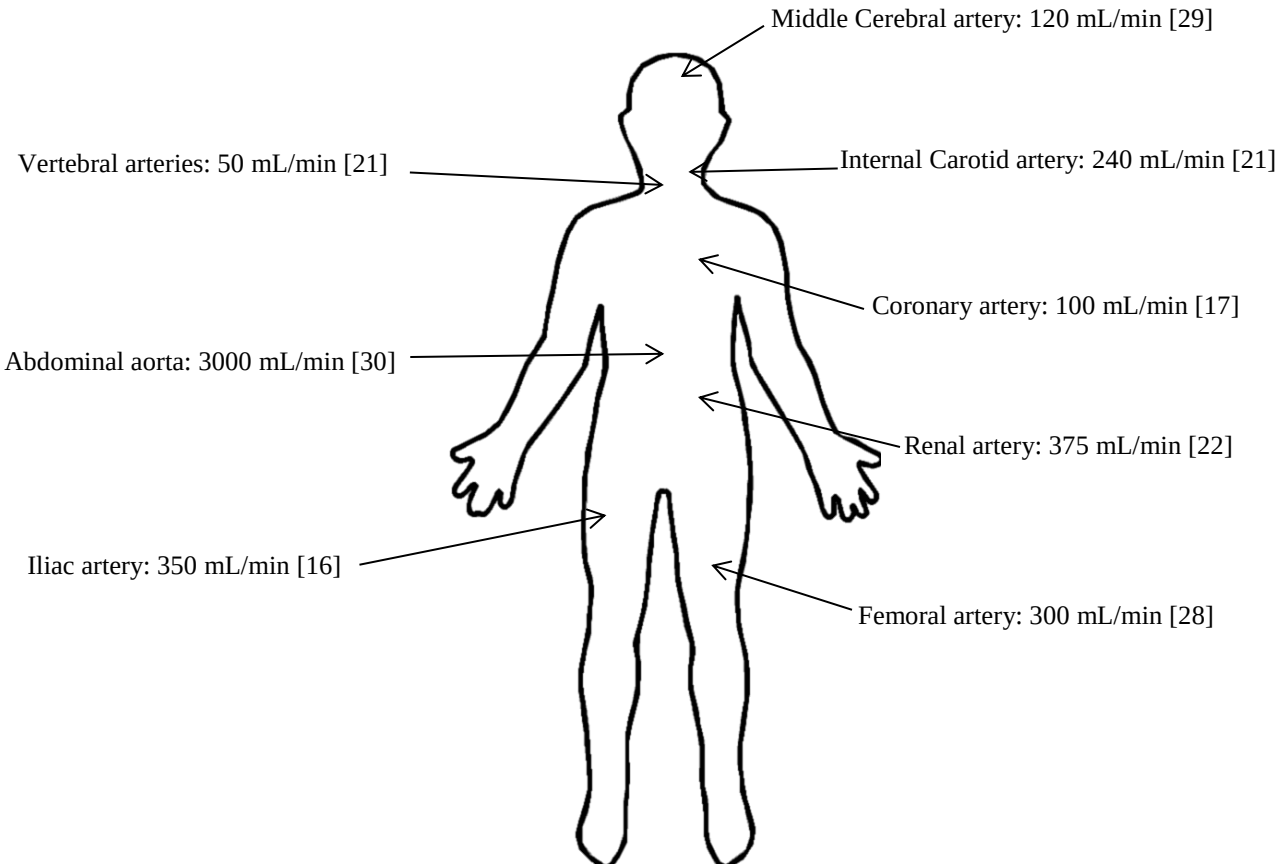

Figure 1: Average measured literature values for blood flow in selected vessels.

Previous studies have focused on these same effects while scanning different types of objects with MR. Many studies [5-10] involved RF heating and coronary stents. Coronary stents are placed directly in the coronary artery and are generally smaller in diameter and length and are therefore less likely to experience significant heating during MRI. This is due to the maximum potential for RF induced heating occurring between the quarter and half RF wavelength of the surrounding medium. Table 1 shows the wavelength of RF waves in different mediums and where the maximum RF induced temperature rise would occur. Coronary stents are typically around 5 cm in length and would not experience worst case scenario heating in a 3.0 T MRI scanner. This study investigates the RF induced heating of a longer stent, one that is indicated for the iliac artery (8 cm) at 3.0 T, to create a worst case scenario to more accurately determine the cooling effects of modeled blood flow. The length of this stent is much closer to the half wavelength resonance value for the strength of magnet used in this study and therefore higher temperature rises would be expected. The wavelength for each is defined as:

$$\lambda = \frac{2\pi}{\omega\sqrt{\frac{\mu\varepsilon}{2}}\sqrt{1+\left(1+\frac{\sigma^2}{\omega^2\varepsilon^2}\right)^{\frac{1}{2}}}} \quad [2]$$

where λ is the wavelength, ω is the angular frequency, μ is the magnetic permeability of the medium, ε is the permittivity of the medium and σ is the electrical conductivity of the medium [25].

Table 1: Frequency and wavelength of RF waves for different MRI field strengths**.**

Field strength (B_o)	Operating frequency (f)	Wavelength in air (λ_a)	Wavelength in tissue (λ_t)	Half wavelength in tissue ($\lambda_t/2$)
0.5 T	21 MHz	14.3 m	160 cm	80 cm
1.5 T	64 MHz	4.7 m	52 cm	26 cm
3.0 T	128 MHz	2.3 m	26 cm	13 cm
7.0 T	299 MHz	1.0 m	11 cm	5.5 cm

Other studies [11] tested heating in non-medical devices such as thin wires and showed general temperature rises in metallic objects exposed to RF induction. The studies found in literature did not investigate the relationship between measured and simulated temperature rises. This study will investigate both experimental and simulation methods of determining RF induced temperature rise and will aim to create a validated tool for accurately predicting RF induced temperature rises of medical devices.

Chapter 3: Methods

Chapter 3i: Experimental Model

Experiments were performed using a gel phantom defined by the current standard test method for evaluating MR safety of medical devices, or ASTM F2182. The gel in the phantom is a mixture of NaCl, polyacrylic acid, and water and it accurately approximates the electrical (conductivity of 0.47 S/m and

permittivity of 80) and thermal parameters (heat capacity of 4150 J/kg°C and diffusivity of 1.3 x 10^{-7} m^2/s) of average human tissue [12]. The phantom was retrofit with a flow channel consisting of a silicone tube with inner diameter of 7.9 mm and outer diameter of 11 mm passing through the length of the phantom. The tubing was connected to a Masterflex L/S peristaltic pump located in the MR equipment room. The pump sent room-temperature water through the tubing at various flow rates. A Zilver 635® Vascular Self-Expanding Stent with a diameter of 10mm and a length of 80mm was then placed around the tubing on the left side of the phantom. The positioning of the stent was chosen as this area has been defined to be the worst case location for RF induced heating [12]. Figure 2 shows where the electric field within the scanner is the highest and the right side of the plot corresponds to the left side of the Siemens scanner used in this study.

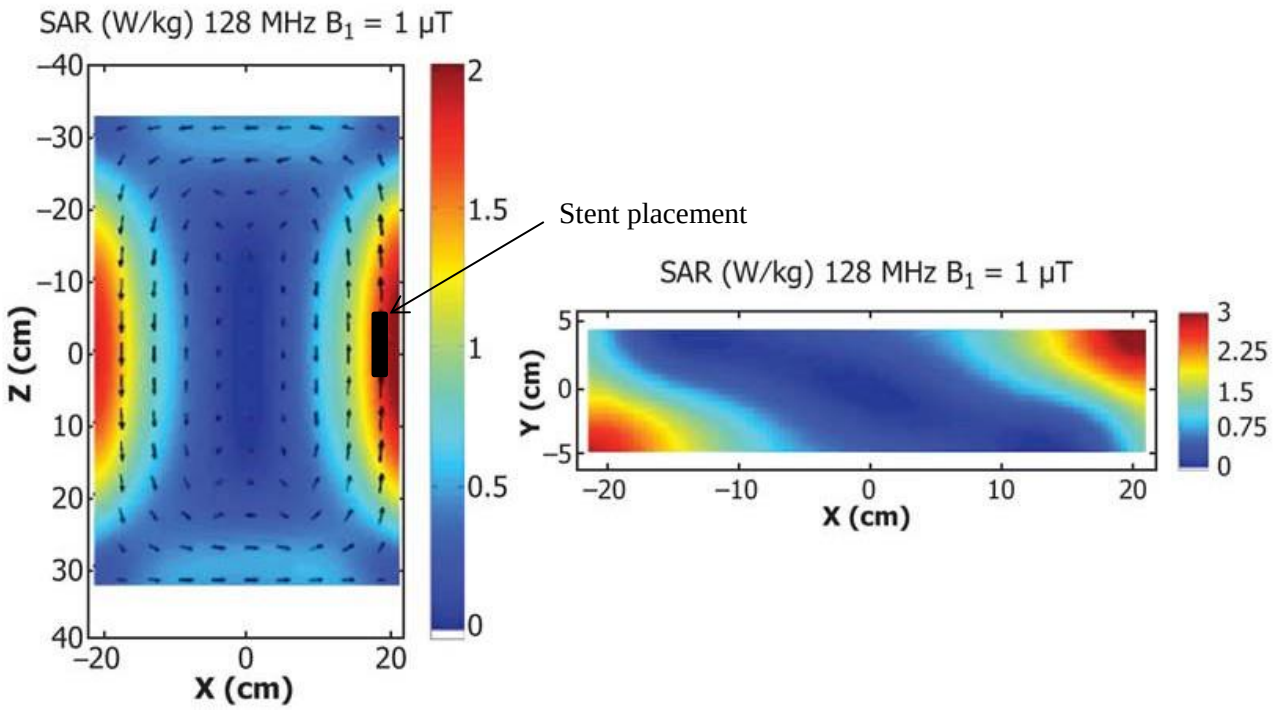

Figure 2: Plot of electric field within 3.0 T MRI scanner and stent placement.

After being expanded and extended along the tubing, the final length of the stent was 95 mm. One fiber-optic temperature probe was then placed on the proximal end of the stent between the stent and the

tubing. Two other probes were placed on the distal end of the stent and in a remote location in the gel but data collected by these probes was not used for this study. In separate trials, the stent and flow channel were removed from the gel phantom and a probe was placed in the same area as the proximal stent probe where transient temperature rises were measured. This setup was utilized for a control study to measure temperature rises of the gel alone. The Zilver stent with fiber optic probes can be seen in figure 3. Figure 4 shows the setup of the phantom outside of the MRI bore. Figure 5 is a schematic of the experimental setup in the scanner room and adjoining equipment room.

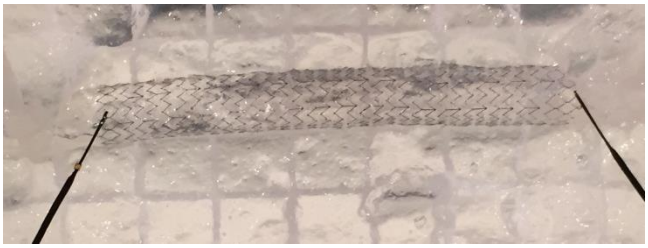

Figure 3: Placement of temperature probes between stent and flow channel tubing.

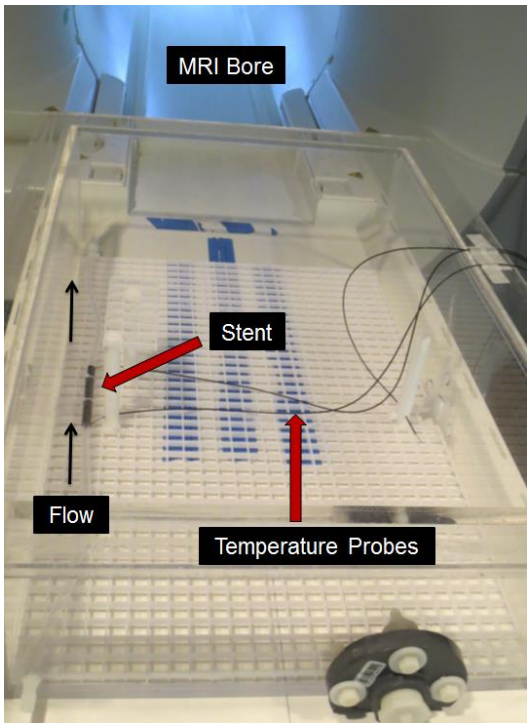

Figure 4: Experimental setup, including empty phantom, vascular stent, flow channel, and temperature probes.

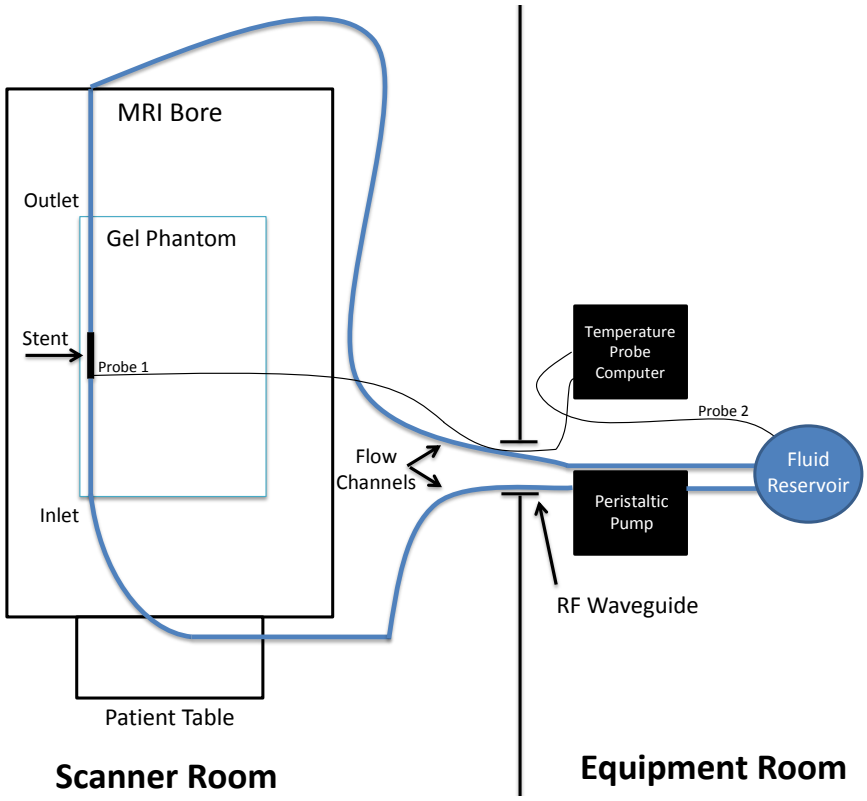

Figure 5: Experimental setup schematic.

The peristaltic pump used to create flow displayed flow rate in terms of revolutions per minute (RPM) of the pump head. The pump head used was a Masterflex peristaltic pump with P/S 18 silicone tubing. Conversion rates were provided by the pump manufacturer and were used to determine the volumetric flow rate for all RPM values. Table 2 shows the volumetric flow rates that were converted from the RPM of the pump head.

Table 2: RPM pump values and corresponding flow rates.

RPM	0	3	4	5	10
mL/Min	0	12	15	19	38
RPM	15	25	50	261	585
mL/Min	58	96	192	1000	2240

All of the trial scans were conducted within a Siemens 3.0 Tesla Tim Trio MRI system. The phantom was registered as a 5’5” female weighing 159 lbs. in the head first, supine position within the

scanner as defined in ASTM F2182 [12]. The RF body coil was used to receive RF signal during scanning. Prior to scanning, the specific absorption rate (SAR), or the normalized rate at which RF power is absorbed by tissue per unit of mass [14], patient protection was turned off in order to reach higher than FDA-allowed SAR values. The SAR value was approximated to be 5.5 W/kg. This increased SAR value creates a worst case scenario where higher temperature rises are expected and therefore allows for more accurate observation of the cooling effects of modeled blood flow. The scans utilized turbo spin echo pulse sequences with flip angles varying from 129° to 131° and a reference amplitude of 600 V.

Scans were then completed using the experimental setup described. Scans utilized 7.5 minute sequences, instead of 15 minutes scans defined in ASTM F2182, while the fiber-optic temperature probes measured transient temperature rises. 7.5 minute scans were utilized for efficiency under the assumption that the rate of RF induced temperature rise of a device begins to slow after the first few minutes of scanning. Each scan was run with a different constant flow velocity (listed in table 2), and each flow velocity was run for 3 trials. Two control scans were also completed that measured the temperature rise of the gel phantom without the stent or flow channel. Data was collected at these varying flow and control rates over a span of 9 separate days. Once each individual scan was completed, the maximum temperature rise was determined and recorded for that particular scan and flow type. The recorded maximum temperature rises were then averaged for each volumetric flow rate.

Chapter 3ii: Simulation Model

COMSOL Multiphysics finite element software was used to simulate the experimental model. The model had been previously created and the experiments conducted in this study were used to validate the COMSOL model. The model coupled electromagnetics, fluid dynamics, and transient heat transfer of RF induced heating of a vascular stent with modeled blood flow. Three nodes in the software were utilized: radio frequency electromagnetic waves, laminar flow, and heat transfer in solids.

The electromagnetic response of the RF coil was solved using Maxwell's wave equation describing propagation of electromagnetic waves through a medium:

$$\nabla \times \mu_r^{-1}(\nabla \times E) - k_o^2\left(\varepsilon_r - \frac{j\sigma}{\omega\varepsilon_o}\right)E = 0 \quad [3]$$

where E is the electric field, μ_r is the relative magnetic permeability, k_o is the initial wave vector, μ_r is the magnetic permeability, ε_r is the relative permittivity, σ is the electrical conductivity, ω is the angular frequency and ε_o is the permittivity of free space [23,24]. The length of the radiofrequency waves was calculated as (identical to equation 2):

$$\lambda = \frac{2\pi}{\omega\sqrt{\frac{\mu\varepsilon}{2}}\sqrt{1+\left(1+\frac{\sigma^2}{\omega^2\varepsilon^2}\right)^{\frac{1}{2}}}} \quad [4]$$

where λ is the wavelength, ω is the angular frequency, μ is the magnetic permeability of the medium, ε is the permittivity of the medium and σ is the electrical conductivity of the medium [25]. The maximum potential for RF induced heating occurs between the quarter and half RF wavelength of the surrounding medium. The heat equation derived from Fourier's law and conservation of energy was used to calculate transient heat transfer:

$$\rho c_p \frac{\partial T}{\partial t} = \nabla\cdot(k\nabla T) + Q \quad [5]$$

where ρ is the density of the gel, c_p is the specific heat capacity of the gel, T is the temperature in the gel, t is the time, k is the thermal conductivity of the gel and Q is the heat source term [26]. It was assumed that convective heat transfer was prevented just as in the experimental case. Q, the source term, was calculated with:

$$Q = \rho SAR = \rho\left(\frac{\sigma|E|^2}{\rho}\right) \quad [6]$$

where ρ is the density of the gel, SAR is the Specific Absorption Rate from the electromagnetic field, σ is the electrical conductivity of the gel, and E is the electric field. The RF field induces an electric current in the stent which generates a local magnetic field. The gel is heated by current losses and then the heat is transferred by equation [3] with the addition of a convective flow term:

$$\rho c_p \frac{\partial T}{\partial t} + \rho c_p u \cdot \nabla T = \nabla \cdot (k \nabla T) + Q \quad [7]$$

where ρ is the density of the fluid, c_p is the specific heat capacity of the fluid, T is the temperature in the fluid and u is the fluid velocity field. The flow through the silicone tubing and stent was modeled as laminar, incompressible flow with no turbulence and a no slip wall condition:

$$\rho(u \cdot \nabla)u = \nabla \cdot [-pI + \mu(\nabla u + (\nabla u)^T)] + F \quad [8]$$

$$\rho \nabla \cdot u = 0 \quad [9]$$

where ρ is the fluid density, u is the fluid velocity, p is the pressure, I is the identity tensor, μ is the dynamic viscosity, T is the total stress tensor for the Newtonian fluid, and F is the resultant force [27].

Table 3 and table 4 show domain values, initial values, boundary conditions, and material properties used in the simulation. The 3.0 Tesla Siemens Tim Trio RF body coil used in the experiment was modeled according to dimensions provided by the manufacturer. The RF body coil was modeled in air as a perfect electrical conductor (PEC) and at a resonance of 123 MHz. This resonance frequency is calculated with:

$$\omega = \gamma B \quad [10]$$

where ω is the resonance frequency, γ is the gyromagnetic ratio, and B is the field strength of the scanner's magnetic bore (B = 2.9 T for the Tim Trio scanner used in the experimental setup). The gel phantom and flow channel were positioned in the simulation to match their experimental positions. The

stent was also modeled as a PEC with linear segments on the outside of the flow channel. The thickness of the silicone tubing was not included in the model. Figure 6 shows the simulation setup of the RF coil, gel phantom with flow channel, and the stent. The three-dimensional domains were meshed with tetrahedral elements and the RF coil and flow channel domains were meshed with triangular elements. The total domain, boundary, and edge elements in the mesh were 626,760, 52,303, and 7,521, respectively. The final computer simulation solved for 3.9 million degrees of freedom in the electromagnetics, 132,000 degrees of freedom in the computational fluid dynamics and approximately 664,000 degrees of freedom in the heat transfer. The average run-time for all simulations was 34 minutes.

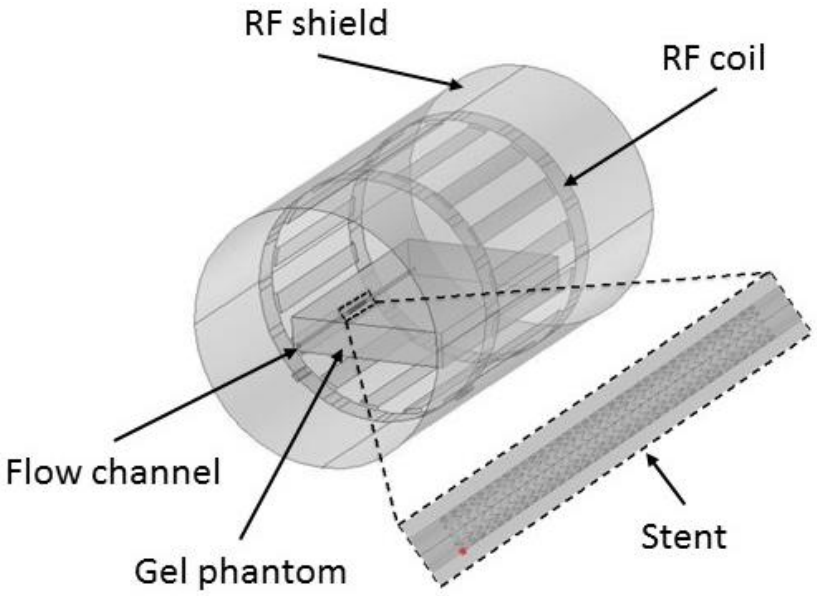

Figure 6: Setup of computer simulation.

Table 3: Domain and input values used in computer model.

Physics	Domains	Initial values	Boundary conditions
Electromagnetics	air sphere RF shield RF coil	$E_{x,y,z} = 0$ V/m	Scattering boundary condition at air sphere: $n \times (\nabla \times E) - jkn \times (E \times n) = -n \times \left(E_o \times \left(jk(n - k_{dir})\right)\right) e^{-jkk_{dir} \cdot r}$ RF shield and coil modeled as Perfect Electrical Conductors (PEC): $n \times E = 0$
Heat transfer	gel in phantom	$T_o = 37$ °C	Thermal insulation on the outer skin of the pig anatomy boundaries: $-n \cdot (-k\nabla T) = 0$
CFD laminar flow	flow channel in the phantom	$p_o = 0$ PA $u_o = 0$ m/s	Normal inflow velocity: $u_o = 100$ cm/s Outlet zero pressure: p = 0 Pa No slip wall condition: u = 0 m/s

Table 4: Thermal and electrical properties of materials used in computer simulation.

Material Properties	Air*	Stent**	Fluid	Gelled Saline
density (kg/m^3)	-	6500	1000	1000
heat capacity (J/(kg·K))	-	320	4200	4150
thermal conductivity (W/(m·K))	-	10	0.6	0.6
viscosity (Pa·s)	-	-	0.9×10^{-3}	-
electrical conductivity (S/m)	0	-	5.5×10^{-6}	0.47
relative permittivity (-)	1	-	80	80
relative permeability (-)	1	-	1	1

*The thermal properties of the air domains were unnecessary for the simulation because the gel phantom was modeled as perfectly insulated.

** The electrical properties of the stent were unnecessary for the simulation because the stent was modeled as a perfect electrical conductor.

Chapter 3iii: Statistical Analysis

A paired t-test was used to determine any significant differences between the maximum temperature rises measured both experimentally and by simulation. The null hypothesis was that no statistically significant difference existed between the experimental and simulation maximum temperature rise at each flow rate. The alternative hypothesis was that the experiment and simulation data differed at each flow rate significantly. A significance level (α) of 0.05 was used. The data was then also analyzed for agreement using a Bland-Altman analysis. The difference between each experimental scan temperature rise and simulated temperature rise for each flow rate was plotted against the mean temperature rise for that flow rate. The resulting plot shows the spread of the data, any resulting bias, and possible outliers [15].

Chapter 4: Results

Figure 7 shows both experimental and simulated transient temperature of the vascular stent plotted over time for no flow and maximum flow cases. Each flow rate resulted in temperature profiles that mimic the overall shape of this plot. Table 5 displays temperature rises measured both experimentally and through the use of the computer simulation for each volumetric flow rate. Table 5 also reports the CEM43 values calculated for flow rate measured experimentally and by simulation. Each experimentally measured temperature rise is an average value of maximum temperature rises collected during multiple trials for each flow rate. No flow (0 mL/min) resulted in an average temperature rise of over 10°C. With a flow rate of only 58 mL/min the average temperature rise was decreased by over 50%. The experimental and computer simulation results are also plotted in figure 8. The simulated temperature rise response of the stent for the no flow case can be seen in figure 9. A paired t-test between the experimental and simulation maximum temperature rises resulted in the null hypothesis not being rejected ($p = 0.24$). Therefore, a statistically significant difference did not exist. The results of the Bland-Altman analysis can

be seen in figure 10. The mean difference of the data was 0.13°C and the upper and lower limits of agreement are 1.21°C and 1.47°C, respectively. The plot also shows three possible outliers, with two being at the highest rate of flow. These outliers existed at temperature rises around 3°C where a standard deviation of 1°C has a larger than expected impact. Standard deviation values of the experimental data are fairly consistent, therefore these outliers are not considered significant.

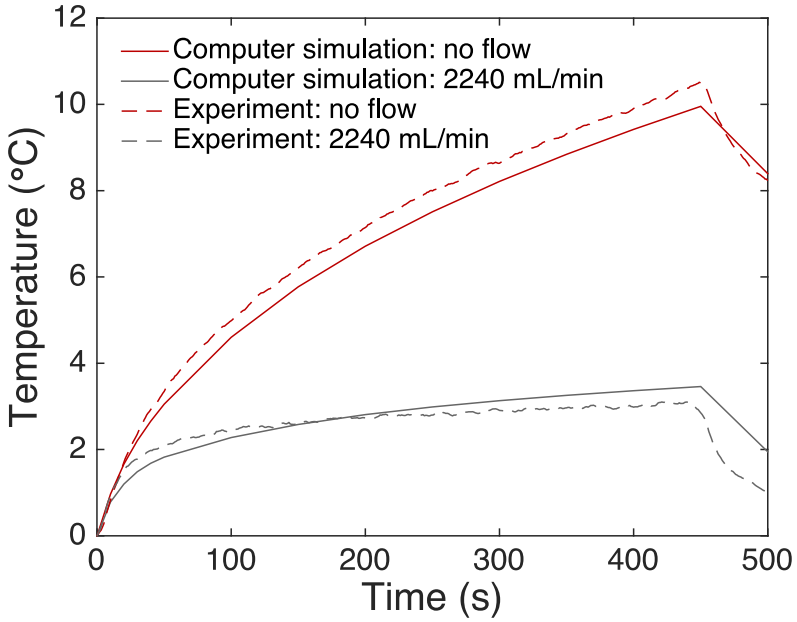

Figure 7: Temperature vs. time for no flow and maximum flow.

Table 5: Experimental and simulation results.

Volumetric Flow Rate (mL/min)	Measured Temperature Rise (°C) (average ± σ)	Simulated Temperature Rise (°C)	Measured CEM43 (min)	Simulated CEM43 (min)
0	10.5 ± 0.7	10.1	45.0	41.1
12	6.6 ± 0.4	6.1	4.3	3.0
15	6.4 ± 0.3	5.9	3.6	2.3
19	6.0 ± 1.0	5.7	2.8	1.9
38	5.6 ± 0.6	5.2	1.6	0.9
58	5.0 ± 0.2	4.9	0.6	0.7
96	4.8 ± 0.5	4.6	0.6	0.5
192	4.2 ± 0.9	4.3	0.6	0.3
1000	3.5 ± 0.3	3.8	0.1	0.2
2240	3.2 ± 1.0	3.6	0.1	0.1
Gel only	3.2 ± 0.3			

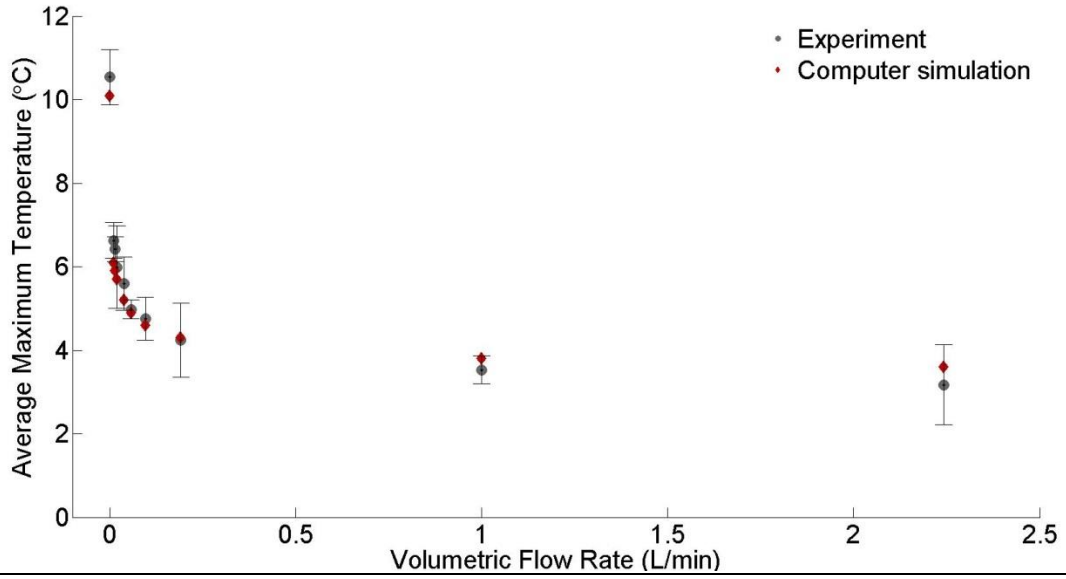

Figure 8: Plot of experimental and computer simulation results.

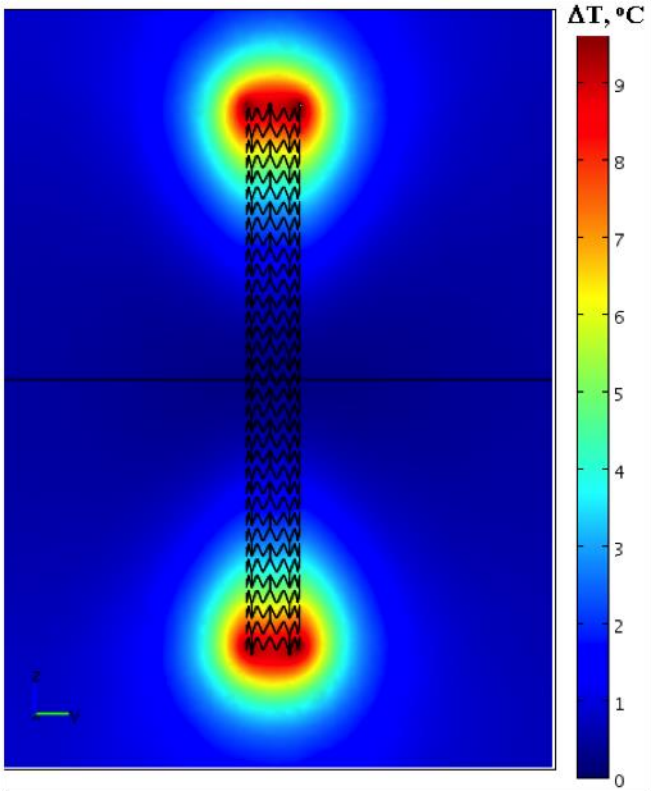

Figure 9: Simulated temperature rise response for no flow case.

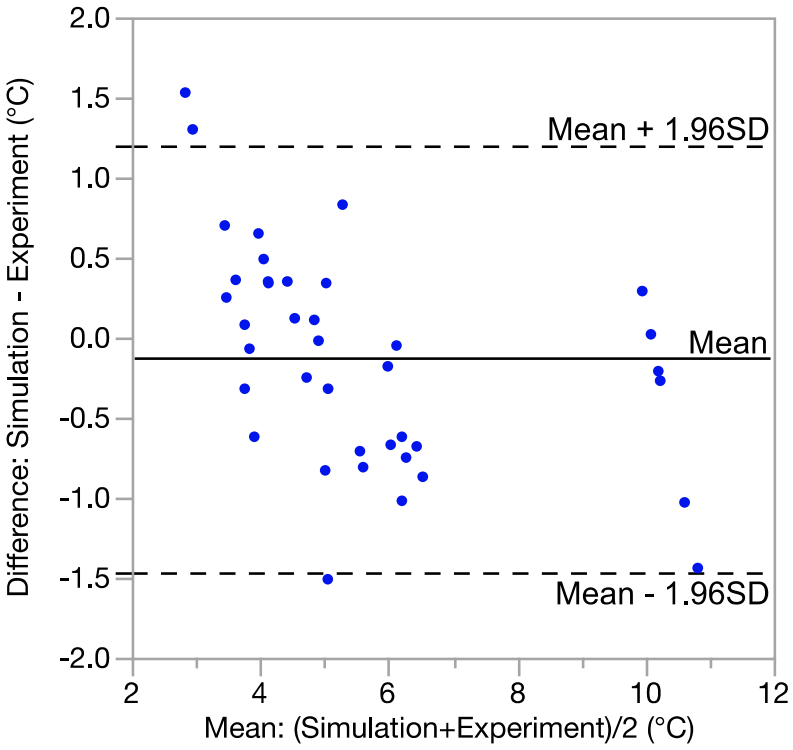

Figure 10: Plot of Bland-Altman analysis results.

Chapter 5: Discussion

Figure 8 shows a clear trend in both the experimental and the computer simulation data. Not only does modeled blood flow have a significant cooling effect on RF induced heating, higher rates of flow reduce temperature rises drastically. Average maximum temperature rise is significantly reduced even at very low flow rates; temperature rises decreased over 50% with only 58 mL/min of flow. The CEM43 value for each flow rate also demonstrates the significant cooling effect of blood flow. The cumulative minutes of exposure decreases by over ten orders of magnitude with only 12 mL/min and continues to drop by nearly 300% as physiologic blood flow ranges are reached. The temperature rises also leveled out after a certain rate of flow. Increasing the flow rate by more than ten times from 196 mL/min to 2240 mL/min resulted in a decrease of only 1.0 and 0.7°C experimentally and in the computer simulation,

respectively. The small change in maximum temperature rise for the high flow rate cases suggests that there is a minimum temperature rise for the stent independent of the flow rate. The control experiment that measured the temperature rise of the gel phantom without the stent or flow channel resulted in a temperature rise of 3.2°C. Therefore, it can be concluded that at higher rates of flow the temperature of the stent is increasing mostly as a result of heating of the gel itself. This trend also suggests that because physiologic blood flow falls within this range [16-17], physiologic RF induced temperature rises will fall somewhere within the range of 3-4°C. The Zilver® stent utilized in this study is indicated for use in the iliac artery where the physiologic blood flow is approximately 350 mL/min [16]. At this rate of flow, the RF induced temperature rise would likely be below 4°C. This study did not account for the effects of capillary perfusion on RF induced temperature rises. Accounting for perfusion would decrease temperature rises even more, as it has been calculated that capillary blood perfusion is capable of reducing temperature rise comparable to blood flow [18].

The statistical analysis resulted in good agreement between the experimental and computer simulation data. A p-value greater than the previously indicated significance level of $\alpha = 0.05$ ($p = 0.24$) resulted in not rejecting the null hypothesis that a statistically significant difference did not exist between the two sets of data. The plot of the Bland-Altman analysis also shows good agreement. A bias (mean difference) of 0.13°C indicates good agreement because the accuracy of the temperature probes is reported as ±0.20°C. The upper and lower limits of agreement of 1.21°C and 1.47°C are also reasonable due to the nature of the variability existing in the experimental setup. Only three possible outliers exist in the data, as they fall outside of the limits of agreement, and two of the points were obtained at the highest rate of flow. The third possible outlier is just outside the lower limit of agreement and is likely a result of experimental variability. The variability along the plot is consistent and the large gap between the two apparent groups of points is indicative of the drastic effect that even a low rate of flow has on RF induced temperature rises.

The Masterflex pump was also tested for accuracy as the manufacturer reports an accuracy of better than 1mL/min. Independent tests involved pumping fluid into a graduated cylinder and recording the time required to reach a certain volume. These tests resulted in a lack of confidence in the pump to be able to accurately achieve very low flow rates. Therefore, measurements for flow rates of less than 12 mL/min were excluded from this report. It was of note, although, that the measurements followed the general trend seen in the data with only slight variations. There were also other idealizations made throughout the study. Laminar flow was used in both the experiment and simulation instead of physiologic pulsating flow. Literature has shown that this idealization is reasonable as there is a negligible difference between the two types of flow in terms of heat flux [19]. The experiments also utilized room temperature fluid and gel because temperature dependent material properties were not expected to be significant over the range of room temperature to human body temperature.

Chapter 6: Conclusion

In conclusion, this study shows the significant cooling effect of flow on RF induced heating of a vascular stent. At physiologic flow rates, temperature rises were reduced by more than 50% of rises for no flow cases. At rates similar to the flow seen in the iliac artery temperature rises were less than 4°C. It is shown that when evaluating the safety of devices it is important to consider the body's natural cooling effects. Patients with certain medical devices that have been withdrawn or restricted from MRI scans may have the potential to receive these scans in the future. The study also presents a validated simulation tool that can accurately predict RF induced temperature rises. There is no significant difference between temperature rises measured experimentally and measured with the use of the simulation. Simulation tools like the one validated with this study can act as tools for scientists that aim to evaluate the MR safety of other medical devices in the future. The simulation can also act as a step toward the use of computer models and simulation of virtual human anatomy. The validated simulation presents a model of an experimental gel phantom and provides groundwork for extending this work to an actual physiology.

Scientists can use validated simulation tools such as the one presented here that mimic responses *in* vivo to further research human responses and eventually create a fully functioning model of the human body.

References

[1] Mozaffarian D, Benjamin EJ, Go AS, et al. Heart disease and stroke statistics—2015 update: a report from the American Heart Association. Circulation 2015;131:e29–e322.

[2] Chen M, Zieve D, Ogilvie I. Angioplasty and Stent Placement - Heart: MedlinePlus Medical Encyclopedia. U.S. National Library of Medicine 2014.

[3] van Rhoon GC, Samaras T, Yarmolenko PS, Dewhirst MW, Neufeld E, Kuster N. CEM 43°C Thermal Dose Thresholds: a Potential Guide for Magnetic Resonance Radiofrequency Exposure levels? European Radiology 2013;23:2215-2227.

[4] ASTM Standard F2503-13. Standard Practice for Marking Medical Devices and Other Items for Safety in the Magnetic Resonance Environment. ASTM International 2013.

[5] Shellock FG, Forder JR. Drug eluting coronary stent: in vitro evaluation of magnet resonance safety at 3 Tesla. J Cardiovasc Magn Reson 2005;7:415–419.

[6] Jost C, Kumar V. Are Current Cardiovascular Stents MRI Safe? J Invasive Cardiol 1998;10:477–479.

[7] Elder NI. Effects of blood flow on the heating of cardiac stents due to radio frequency fields. West Lafayette, IN; 2013.

[8] Santoro D, Winter, L, Müller A. Detailing Radio Frequency Heating Induced by Coronary Stents: A 7.0 Tesla Magnetic Resonance Study. PLoS ONE 2012;7(11).

[9] Nyenhuis J, Elder N, Hossainy S. Reduction due to coronary blood flow of stent heating induced by the RF Magnetic Field during MRI. In: Washington, DC; 2015.

[10] Chou CK, McDougall J, Chan, K. RF Heating of Implanted Spinal Fusion Stimulator During Magnetic Resonance Imaging. IEEE Transactions on Biomedical Engineering 1997;44(5):367-373.

[11] Bassen H, Kainz W, Mendoza G, Kellom T. MRI-Induced Heating of Selected Thin Wire Metallic Implants-- Laboratory and Computational Studies-- Findings and New Questions Raised. Minim Invasive Ther Allied Technol 2006;15:76–84.

[12] ASTM Standard F2182-11a. Standard Test Method for Measurement of Radio Frequency Induced Heating On or Near Passive Implants During Magnetic Resonance Imaging. ASTM International 2011.

[13] Cole Parmer® "Masterflex L/S Easy-Load II Head for Precision Tubing, PPS/SS: Flow Chart".

[14] Shellock F, Crues J. MR Procedures: Biologic Effects, Safety, and Patient Care1. Radiology 232.3 (2004): 635-52.

[15] Bland MJ, Altman DG. Statistical Methods for Assessing Agreement Between Two Methods of Clinical Measurement. Lancet 1986;327:307-310.

[16] Strandness DE, Sumner DS. Hemodynamics for Surgeons. New York: Grune & Stratton; 1975.

[17] Klocke FJ. Coronary Blood Flow in Man. Prog Cardiovasc Dis 1976;19:117-166.

[18] Nyenhuis J, Elder N, Hossainy S. Reduction Due to Coronary Blood Flow of Stent Heating Induced by the RF Magnetic Field During MRI. BMESFDA Frontiers in Medical Devices Conference Innovations in Modeling and Simulation 2015.

[19] Craciunescu OI, Clegg ST. Pulsatile Blood Flow Effects on Temperature Distribution and Heat Transfer in Rigid Vessels. J Biomech Eng 2001;123:500-505.

[20] Young DB. Control of Cardiac Output. San Rafael (CA): Morgan & Claypool Life Sciences; 2010. Chapter 1, Introduction.

[21] Oktar SO, Yücel C, Karaosmanoglu D, et al. (2006). Blood-flow volume quantification in internal carotid and vertebral arteries: comparison of 3 different ultrasound techniques with phase-contrast MR imaging. American journal of neuroradiology, 27(2), 363-369.

[22] Savader SJ, Lund GB, & Osterman FA. (1997). Volumetric evaluation of blood flow in normal renal arteries with a Doppler flow wire: a feasibility study. Journal of vascular and interventional radiology, 8(2), 209-214.

[23] Tipler PA, Mosca G. Physics for Scientists and Engineers, Volume 2: Electricity, Magnetism, Light, and Elementary Modern Physics. Macmillan; 2004.

[24] Maxwell JC. A Dynamical Theory of the Electromagnetic Field. Philosophical Transactions of the Royal Society of London 1865;155:459–512.

[25] Yeung CJ, Susil RC, Atalar E. RF safety of wires in interventional MRI: using a safety index. Magn Reson Med 2002;47:187–193.

[26] Cannon JR. The One-Dimensional Heat Equation. Cambridge University Press; 1984.

[27] Incropera FP, Lavine AS. Fundamentals of Heat and Mass Transfer. John Wiley & Sons; 2011.

[28] Holland CK, Brown JM, Scoutt LM, Taylor KJ. (1998). Lower extremity volumetric arterial blood flow in normal subjects. Ultrasound in medicine & biology, 24(8), 1079-1086.

[29] Stock KW, Wetzel SG, Lyrer PA, Radü EW. (2000). Quantification of blood flow in the middle cerebral artery with phase-contrast MR imaging. European radiology, 10(11), 1795-1800.

[30] Taylor CA, Cheng CP, Espinosa LA, Tang BT, Parker D, Herfkens RJ. (2002). In vivo quantification of blood flow and wall shear stress in the human abdominal aorta during lower limb exercise. Annals of biomedical engineering, 30(3), 402-408.

[31] Yarmolenko PS, Moon EJ, Landon C, Manzoor A, Hochman DW, Viglianti BL, Dewhirst MW. Thresholds for thermal damage to normal tissues: an update. Int J Hyperthermia 2011;27:320–343.

[32] van Rhoon GC, Samaras T, Yarmolenko PS, Dewhirst MW, Neufeld E, Kuster N. CEM43°C thermal dose thresholds: a potential guide for magnetic resonance radiofrequency exposure levels? Eur Radiol 2013;23:2215–2227.